Supplementary Information

1 Description of the Mathematical Modelling

1.1 Two-State Model of Bacterial Chemotaxis

The mathematical description used in this work to simulate the dynamics of a chemotactic signalling system relies on following assumptions:

1. The numbers of protein copies are sufficiently large, such that stochastic effects on the protein level can be neglected
2. Each stable receptor complex includes one kinase protein, CheA.
3. A receptor complex can exist only in two functional states, active or inactive (two-state model) [1]
4. The rate of CheA phosphorylation is assumed to be proportional to the average number of active receptor complexes in the cell
5. The protein-protein interaction can be described by Michaelis-Menten kinetics

The probability, $p_m(L)$, of receptor in methylation state $m \in \{0, 1, 2, 3, 4\}$ to be active in an ambient chemo-attractant concentration L is given by

$$p_m(L) = V_m \left(1 - \frac{L^{H_m}}{L^{H_m} + K_m^{H_m}}\right) \tag{S1}$$

The response amplitudes, V_m, Hill coefficients, H_m, and the values at half maximum response, K_m, used throughout this work are taken from Ref. [2] and are listed in Table S1.

We emphasise that none of the results derived in this work depends on the precise values of these coefficients.

Sites methylated	$K_m[mM]$	H_m	V_m
0	$27 \cdot 10^{-4}$	1.2	0.0
1	$20 \cdot 10^{-3}$	1.2	0.25
2	$150 \cdot 10^{-3}$	1.2	0.5
3	$150 \cdot 10^{-2}$	1.2	0.75
4	60	1.2	1

Table S1: Parameters for response of receptors in different methylation states to chemo-attractant (α-methyl-DL-aspartate).

The time-evolution of the different phosphorylation and methylation states for the *E. coli* topology (Fig. 1c) follows along the lines of Rao et al (c.f. Ref. [3]) and are described by the equations

$$\begin{aligned}
\partial_t T_m &= k_R R \frac{T_{m-1}}{K_R + T^T} + k_B\, p_{m+1}(L) Bp\, \frac{T_{m+1}}{K_B + T_A} \\
&\quad - k_R R \frac{T_m}{K_R + T^T} - k_B\, p_m(L) Bp\, \frac{T_m}{K_B + T_A} \qquad \text{(S2)} \\
\partial_t Ap &= k_A \left(A^T - Ap\right) T_A - k_Y Ap \left(Y^T - Yp\right) \\
&\quad - k'_B Ap \left(B^T - Bp\right) \qquad \text{(S3)} \\
\partial_t Yp &= k_Y Ap \left(Y^T - Yp\right) - k_Z Yp\, Z \qquad \text{(S4)} \\
\partial_t Bp &= k'_B Ap \left(B^T - Bp\right) - \gamma_B Bp\,, \qquad \text{(S5)}
\end{aligned}$$

where k_R and k_B are the methylation and demethylation rates and K_R and K_B the corresponding Michaelis-Menten constants, respectively. The concentration of receptor complexes with m residues methylated are denoted by T_m and $T_A = \sum_m p_m(L)\, T_m$ is the concentration of active receptors. All other protein concentrations are denoted as in the main text. The equations of the topologies Fig. 1a-1d are set up in a similar way as Eqs. (S2-S5). It has been shown for *E. coli in vitro* [4] and *in vivo* [2] that changing an attractant occupancy of just a few receptors out of thousands elicits a much larger change in kinase activity. There is increasing evidence that this signal amplification (gain) in bacterial chemotaxis can be explained by long-range allosteric interactions between receptors localized at the cell poles [5, 6, 7, 8, 9, 10]. To account for the receptor interactions in a simple way, we assume that kinase activity depends linear on the concentration of all active receptors. Thus, the first term in Eq. S4 does not reflect a bimolecular reaction but accounts for the strong non-linear relation between receptor occupancy with chemo-ligand and kinase activity in a mean field approximation [10].

The average concentrations of the chemotaxis proteins are taken from Ref. [11] for the strain RP437 assuming a cell volume of 1.4 fl: [CheA]= 5.3 μM, [CheY]= 9.7 μM, [CheB]= 0.28 μM, [CheR]= 0.16 μM, [CheZ]= 3.8 μM. The concentration of the receptor complexes is set equal to [CheA]. The expression levels in the FRET experiments Fig. 3b were estimated to be 18μM for CheY-YFP and 8μM for CheZ-CFP [12, 13].

1.2 Determination of kinetic constants used in simulations.

The kinetic rates and Michaelis-Menten constants of the methylation process are determined such that the maximum number of bacteria in a population show accurate chemotactic response under physiological intercellular variations in protein concentrations as measured in Fig. 2. The protein concentrations for the individuals in a population are generated by the random process

$$x_i = \langle x_i \rangle \left(\lambda r_{ex} + \nu \sqrt{\lambda r_{ex}}\, \xi_i^{(2)} \right) \quad , \tag{S6}$$

with x_i the protein concentrations of the i-th chemotaxis protein and $\langle x_i \rangle$ the corresponding mean concentration of x_i for the strain RP437, as given before. The factor of overexpression is denoted by λ. The co-variations follow a log-normal distribution given by $r_{ex} = N_r \exp[\alpha\, \xi^{(1)} \ln 10]$ with N_r chosen such that $\langle r_{ex} \rangle = 1$, and $\xi^{(1)}$ and $\xi^{(2)}$ are normally distributed random variables with mean zero and variance one. The values $\nu = 0.20$, $\alpha = 0.20$ reproduce intrinsic and extrinsic noise measured in Fig. 2a and Fig. 2b, respectively (see also Fig. S1). The decrease of the intrinsic noise with $\eta_{in} \sim (\lambda r_{ex})^{-1/2}$ assumes that translation follows a Poisson process and proteins are expressed from polycistronic mRNA (see Ref. [14]). This is confirmed by co-expression of CheY-YFP and CheZ-CFP as a single transcript from a plasmid (pVS88) at different levels of IPTG induction (Table S2 and Fig. S2). The population size used in the simulations are 70 individuals for the determination of the kinetic constants and 10^4 individuals for quantifying the fraction of chemotactic bacteria (Fig. 3 and Fig. 4).

The following rate constants are estimated from various measurements found in the literature [15]. The CheA autophosphorylation rate mediated by active receptors is set to $k_A = 50\mu\mathrm{M}^{-1}s^{-1}$. The CheY phosphorylation by phosphotransfer from CheA to CheY has the value $k_Y = 100\mu\mathrm{M}^{-1}s^{-1}$. The dephosphorylation rate for CheY are given by $k_Z = 30/[\mathrm{CheZ}]\mathrm{s}^{-1}$ and $\gamma_Y = 0.1$ for the topologies Fig. 1b, 1c, 1d and $\gamma_Y = 30.1$ for topology

n	η_{ex}	η_{in}	$\eta_{in}^{theo} = \eta_{in}^{wt} n^{-1/2}$
1	0.44	0.20	0.20
2.52	0.27	0.15	0.13
14.1	0.21	0.067	0.053

Table S2: Intrinsic and extrinsic noise of CheY-YFP and CheZ-CFP expression from a single IPTG-inducible promoter at 0μM, 5μM, and 10μM IPTG. Mean expressions are denoted by n. The extrinsic and intrinsic noise, η_{ex} and η_{in}, decline for higher expression level and latter agrees with the intrinsic noise predicted from the model Eq. (S6), $\eta_{in}^{theo} = \nu n^{-1/2}$, with $\nu = 0.20$ the intrinsic noise of the wild type.

Fig. 1a. For the topologies Fig. 1c, 1d the optimal value for [CheBp] can be determined from an optimisation procedure for highest chemotactic performance as described below, but the outcome is essentially that CheBp takes the smallest possible value (see section 3.4). We therefore adjust the rate of CheB phophorylation such that [CheBp] is about one fourth the total concentration of CheB. Furthermore, for CheB activation we set $k'_B = 3\mu\mathrm{M}^{-1}s^{-1}$ with corresponding auto-dephosphorylation rate $\gamma_B = 1s^{-1}$.

The rate constants for the methylation process are determined by computer simulations with parameters given above to result in an adaptation time of 100s after sudden addition of chemo-attractant (35μM) and an adaptation time of 25s after removal. Further conditions are an adapted concentration of phosphorylated CheY to one third its total value. We determine the optimal rate and Michaelis-Menten constants by minimising the quadratic functional

$$E[\mathbf{k}, \mathbf{K}] = \min \frac{1}{N} \sum_{i=1}^{N} \left[\sum_{l=1}^{N_L} \frac{\left(Yp_l^{(i)} - Yp^*\right)^2}{N_L {\sigma_Y}^2} + \frac{\left(\tau_1^{(i)} - \tau_1^*\right)^2}{2{\sigma_1}^2} + \frac{\left(\tau_2^{(i)} - \tau_2^*\right)^2}{2{\sigma_2}^2} \right] \tag{S7}$$

with $\tau_1^* = 100s$, $\tau_2^* = 25s$, and $Yp^* = 1/3\, Y^T$. Because precise adaption is the outstanding feature of the chemotaxis pathway it is reasonable to assume that a higher selective pressure is given for the precise regulation of CheYp than of adaptation times. In the simulations we use the standard deviations, $\sigma_Y = 1/6\, Yp^*$, $\sigma_1 = 1/2\, \tau_1^*$ and $\sigma_2 = 1/2\, \tau_1^*$ but for the general conditions that σ_Y/Yp is significantly smaller than σ_1/τ_1^* and σ_2/τ_2^* we arrive essentially at the same results as for the specific standard deviations above (data not shown). The sum runs over N individuals whose protein concentration are generated from the random process, Eq. (S6), and $N_L = 3$ denotes the

number of stepwise increments of chemo-attractant to show maximum response.

The result of the optimisation procedure for the different topologies in Fig. 1 is given in Table S3. For the additional CheY-receptor feedback in topology Fig. 1d we follow along the lines of Ref. [3]. The CheY-CheZ feedback is modelled by introducing a Hill coefficent for this reaction. Latter is found to be very close to one after optimisation.

Topology	k_R	K_R	k_B	K_B
Fig. 1a	0.5	0.062	16	16
Fig. 1b	1.0	0.043	16	10.1
Fig. 1c	0.39	0.099	6.3	2.5
Fig. 1d	0.4	0.063	6.4	2.5

Table S3: Kinetic constants of the methylation process for the different topologies Fig. 1. The rate constants, k_R and k_B, are given in units of $\mu M^{-1} s^{-1}$ and the Michaelis-Menten constants, K_R and K_B, are given in units of μM.

2 Robustness against Variations in Transcriptional Activity

In this section we derive the necessary conditions for a chemotaxis pathway in order to be robust against variations in transcriptional activity. Transcriptional noise leads to co-variation of expression-levels within the same operon, as shown in Fig. 2b, Figs. S1 and S1, and Table S2. The extend of these covariations can increase up to ten-fold of the wild type gene expression [11]. Bacterial populations showing chemotactic response among all their individuals are more likely to survive in a competing environment than bacteria which lose their chemotactic ability under such variations in gene expression. Thus, the topology of the chemotaxis pathway should have evolved in such a way that the steady state concentration of the response regulator protein CheYp is invariant under a λ-fold increase in transcriptional activity.

The time evolution of a spatial homogeneous biochemical network can be described by a set of ordinary differential equations. Let $\{y_1(t), \ldots, y_N(t)\}$ be the concentrations of the N different states of the proteins involved in the pathway. Summation over all different states of the protein with index k results in the total concentration $x_k^T = \sum_{\{y_i\}_k} y_i$. Since the dynamics of the chemotaxis pathway ranges on time scales from 10^{-2} seconds to minutes, and the turnover time for proteins is significantly larger in bacteria, we can assume the total concentration of the chemotactic proteins to be constant, i.e. $\partial_t x_k^T = 0$.
Thus, the differential equations describing the dynamics of the chemotaxis pathways shown in Fig. 1 have the functional form

$$\partial_t y_i(t) = F_i(\mathbf{y}(t)|\mathbf{x}^T) \tag{S8}$$

The steady state solution $F_i(\mathbf{y}(t)|\mathbf{x}^T) = 0$ of this system is invariant under a λ-fold increase of transcriptional activity $\mathbf{x}^T \rightarrow \lambda\mathbf{x}^T$ if it satisfies the homogeneity condition

$$F_i(\mathbf{y}(t)|\lambda\mathbf{x}^T) = \lambda^{\mu_i} F_i(\mathbf{y}(t)|\mathbf{x}^T), \tag{S9}$$

with $\mu_i \in \{1, 2, 3 \ldots\}$. For the chemotaxis topologies depicted in Fig. 1, we have $\mu_i = 1$ for all i. In the following we identify the topological features of a chemotaxis pathway in order to be invariant against variations in transcriptional activity.

We first investigate the Barkai-Leibler system shown in Fig 1a. To illustrate the point we assume that each receptor has only one methylation

site. Methylated receptors are active with probability $p(L)$ with L the ambient ligand concentration. Non-methylated receptors remain inactive with probability one. The set of differential equations for this system is given by

$$\begin{aligned}
\partial_t T_M &= k_R R^T \frac{T^T}{K_R + T^T} - k_B B \frac{T_A}{K_B + T_A} && \text{(S10)}\\
&\approx k_R R^T - k_B B^T \frac{T_A}{K_B + T_A} && \text{(S11)}\\
\partial_t Ap &= k_A T_A \left(A^T - Ap\right) - k_Y Ap \left(Y^T - Yp\right) && \text{(S12)}\\
\partial_t Yp &= k_Y Ap \left(Y^T - Yp\right) - \gamma_Y Yp \, . && \text{(S13)}
\end{aligned}$$

The approximation resulting in Eq. (S11) is valid for $T^T \gg K_R$, i.e. for R working at saturation. Also, we assume that only active receptors can be demethylated. The dephosphorylation rate of $CheYp$ is given by γ_Y.
The steady state concentrations of the active components of this system are:

$$\begin{aligned}
T_A &= K_B \frac{k_R R^T}{k_B B^T - k_R R^T} && \text{(S14)}\\
Ap &= \frac{k_A T_A A^T}{k_A T_A + k_Y \left(Y^T - Yp\right)} \approx \frac{k_A T_A}{k_Y} \cdot \frac{A^T}{Y^T} && \text{(S15)}\\
Yp &= \frac{k_Y Ap\, Y^T}{k_Y Ap + \gamma_Y} && \text{(S16)}
\end{aligned}$$

Approximations made in Eq. (S15) are valid for $Y^T \gg Yp$ and $k_Y Y^T \gg k_A T_A$. Latter is equivalent to $A^T \gg Ap$, which means that the phosphotransfer from $CheAp$ to $CheY$ is significantly faster than the autophosphorylation of $CheA$. Performing the transformation $\mathbf{x}^T \rightarrow \lambda \mathbf{x}^T$on Eqs. (S14)-(S15) shows that the steady state concentration of the active form of the receptor T_A and of $CheAp$ remain unchanged, since we can eliminate λ in these equations. But in Eq.(S16), λ cannot be eliminated. Thus the steady state concentration of $CheYp$ increases with λ. This means that the Barkai-Leibler model shown in Fig.1a is not robust against variations in transcriptional activity.
For topologies Fig. 1b-1d there is a phosphatase $Z = [CheZ]$ that dephosphorylates activated $CheY$. For these topologies the dephosphorylation term of $CheYp$ is given by $\gamma_Y Yp = k_Z Z^T Yp$. Therefore Eq.(S13) can be rewritten as:

$$\partial_t Yp = k_Y Ap \left(Y^T - Yp\right) - k_Z Z^T Yp \qquad \text{(S17)}$$

This changes the steady state equation of $CheYp$ to:

$$Yp = \frac{k_Y Ap\, Y^T}{k_Y Ap + k_Z Z^T} = \frac{k_Y Ap}{k_Z} \cdot \frac{Y^T}{Z^T} \qquad \text{(S18)}$$

The approximation made here is valid for $k_Z Z^T \gg k_Y Ap$, which is equivalent to $Y^T \gg Yp$. Now the transformation $\mathbf{x}^T \to \lambda \mathbf{x}^T$ leaves the steady state of $CheYp$ unchanged. So in order to be robust against variations in transcriptional activity, $CheYp$ has to have a phosphatase.

For topologies Fig. 1c, 1d the methylesterase $CheB$ is only active if it is phosphorylated by Ap. Thus for these topologies we get an additional differential equation for $Bp = [CheBp]$ given by

$$\partial_t Bp \;\; = \;\; k'_B \, Ap \, \left(B^T - Bp \right) - \gamma_B Bp \, , \tag{S19}$$

with k'_B the rate of phophotransfer from CheAp to CheB and γ_B is the dephosphorylation rate of Bp. Technically the term $k'_B \, Ap \, \left(B^T - Bp \right)$ has to be considered also in Eq.(S12). But since $k_Y Y^T \gg k'_B \, B^T$, this term can be neglected. Then the steady state of this equation reads:

$$Bp \; = \frac{k'_B Ap \, B^T}{k'_B Ap + \gamma_B}. \tag{S20}$$

Under the transformation $\mathbf{x}^T \to \lambda \mathbf{x}^T$ the steady state value for Bp increases by a factor λ. For the receptor activity to be invariant against transcriptional noise, the scaling of $CheBp$ with λ is a necessary condition, as can be seen from Eq. (S14).
Clearly, if $CheBp$ would have a phosphatase, it would not scale with λ. This in turn would destroy the invariance of T_A. As a result, neither $CheAp$ nor $CheYp$ would be invariant under λ-fold increase in protein levels.

Also, an auto-methylation process of the receptors is no alternative to the methyltransferase $CheR$. Assuming auto-methylation as the main methylation process, we would have to substitute the term $k_R R^T$ in Eq. (S11) by $k_m(T^T - T^A)$, with k_m the automethylation rate. But then the homogeneity condition, Eq. (S9), would be violated.

Summarising we can say that in order for a topology to be robust against variations in transcriptional activity, the following conditions have to be fulfilled:

- a methyltransferase $CheR$ has to exist and work at saturation,
- the dephosphorylation of $CheYp$ has to be taken over by a phosphatase $CheZ$, see Eq.(S18),
- $CheBp$ must not have a phosphatase
- $CheAp$ and $CheYp$ have to be significantly smaller than their total concentrations, i.e. $Ap \ll A^T$ and $Yp \ll Y^T$.

So far we have shown that the steady states of topologies Fig. 1b-1d are robust against variations in transcriptional activity. But what happens to the dynamics of a system under this transformation? Since the differential Eqs.(S11), (S12), (S17) and (S19) are linear in the concentrations $\{A^T, B^T, R^T, Y^T\}$ under the assumptions $A^T \gg Ap$, $Y^T \gg Yp$, the entire system $F_i(\mathbf{y}(t)|\mathbf{x}^T)$ is a linear function with respect to $\mathbf{x}^T$ and we can write:

$$\partial_t y_i = F_i(\mathbf{y}(t)|\lambda\mathbf{x}^T) = \lambda F_i(\mathbf{y}(t)|\mathbf{x}^T) = \lambda\partial_{t'} y_i \tag{S21}$$

This means, a λ-fold increase in transcriptional activity results in a rescaling of time: $t' = \lambda t$. Now the dynamics of both systems are identical in different time-frames. Temperature changes, e.g., alter kinetic rate constants and result to first order also in a rescaling of time. Consequently the steady state values of the pathway are also invariant under moderate variations in the ambient temperature.

3 Error Reduction Mechanisms

In this section we show how errors on the output signal arising from imperfection of components or independent variations of protein levels can partially be compensated by additional feedback loops and an optimal choice of kinetic parameters. In the following we look at the differential equations of the topologies of *E. coli* and the Barkai-Leibler system to show the difference in error reduction between topologies with and without additional feedback.
The differential equations for the topology in Fig. 1c for the receptor methylation T_M, the receptor protein $Ap = [CheAp]$, the messenger protein $Yp = [CheYp]$, and the methylesterase $Bp = [CheBp]$ are given by

$$\begin{aligned}
\partial_t T_M &= k_R R^T - k_B Bp \frac{T_A}{K_B + T_A} && \text{(S22)}\\
\partial_t Ap &= k_A \left(A^T - Ap\right) T_A - k_Y Ap \left(Y^T - Yp\right) \\
&- k'_B Ap \left(B^T - Bp\right) && \text{(S23)}\\
\partial_t Yp &= k_Y Ap \left(Y^T - Yp\right) - k_Z Yp\, Z, && \text{(S24)}\\
\partial_t Bp &= k'_B Ap \left(B^T - Bp\right) - \gamma_B Bp\,. && \text{(S25)}
\end{aligned}$$

In this topology, the demethylation of the receptor complex is performed only by the phosphorylated form of $CheB$. The phosphorylation of $CheB$ is done by the phosphordonor $CheAp$ of the receptor complex. Thus the activated form of $CheB$ is a function of the activity of the receptor complex, and one has the functional form $Bp = Bp\,(Ap\,)$. This functional dependence gives an additional feedback to the system as shown in Fig. 1c.
For the Barkai-Leibler system, topology Fig.1a, the methylesterase of the receptor complex is active only in unphosphorylated form and does thus not depend on the phosphorylation level of $CheA$, see Eqs. (S11)-(S13).
From the steady state of Eq.(S23) we can define the functional:

$$\begin{aligned}
f\,(Ap\,, Bp\,, Yp\,, T_A) \;:=\; & k_A \left(A^T - Ap\right) T_A - k_Y Ap \left(Y^T - Yp\right) \\
& - k'_B Ap \left(B^T - Bp\right), && \text{(S26)}
\end{aligned}$$

where the functions $T_A = T_A(Bp\,, R)$, $Yp = Yp\,(Ap\,, Z)$ and $Bp = Bp\,(Ap\,)$ are derived from the steady states of Eqs.(S22),(S24) and (S25). We calculate the total differential of the functional f to get the sensitivity of the kinase activity of $CheAp$ with respect to changes in protein concentrations.

To get the dependence of Ap and R to linear order, one has to calculate the total differential of the functional in Eq.(S26)

$$df = \frac{\partial f}{\partial Ap} dAp + \frac{\partial f}{\partial R} dR = 0, \qquad \text{(S27)}$$

keeping all other protein concentrations constant. Solving this for dAp gives:

$$\begin{aligned} dAp &= -\left(\frac{\partial f}{\partial Ap}\right)^{-1}\frac{\partial f}{\partial R}dR \\ &= -\frac{\frac{\partial f}{\partial T_A}\frac{\partial T_A}{\partial R}}{\left.\frac{\partial f}{\partial Ap}\right|_{T_A,Yp,Bp} + \frac{\partial f}{\partial Yp}\frac{\partial Yp}{\partial Ap} + \left(\frac{\partial f}{\partial T_A}\frac{\partial T_A}{\partial Bp} + \left.\frac{\partial f}{\partial Bp}\right|_{T_A}\right)\frac{\partial Bp}{\partial Ap}}dR \end{aligned} \tag{S28}$$

The terms after the vertical lines indicate the concentrations kept constant for this derivative. Using the following definitions:

$$\alpha := \left.\frac{\partial f}{\partial Ap}\right|_{T_A,Yp,Bp} + \frac{\partial f}{\partial Yp}\frac{\partial Yp}{\partial Ap} \tag{S29}$$

$$\beta := \left.\frac{\partial f}{\partial Bp}\right|_{T_A} + \frac{\partial f}{\partial T_A}\frac{\partial T_A}{\partial Bp}, \tag{S30}$$

we can simplify the representation of dAp to:

$$dAp = \frac{\frac{\partial f}{\partial T_A}\frac{\partial T_A}{\partial R}}{\alpha + \beta\frac{\partial Bp}{\partial Ap}}dR \tag{S31}$$

The term $\partial Bp/\partial Ap$ arises through the additional feedback and is zero for the Barkai-Leibler topology. In section 3.1 we show that α is always negative for $Y^T \gg Yp$. In section 3.2 we show that β is always negative for K_B being sufficiently large. Since $\partial Bp/\partial Ap > 0$, what can be seen from the steady state of Eq.(S25), the absolute value of the denominator of Eq.(S31) is larger for the topology with additional feedback than for the Barkai-Leibler model. This means, that fluctuations in the activity of $CheAp$, that result from fluctuations of $CheR$, are minimised by the additional feedback loop. The error reduction by this additional feedback loop works better, the greater the term $\beta\partial Bp/\partial Ap$ is. As shown in section 3.4, the effectiveness of the error correction of the feedback increases with B^T/Bp.
Equivalently, these calculations can be done for the other proteins concentrations , resulting in:

$$dAp = -\frac{\frac{\partial f}{\partial T_A}\frac{\partial T_A}{\partial R}}{\alpha+\beta\frac{\partial Bp}{\partial Ap}}dR \tag{S32}$$

$$dAp = -\frac{\frac{\partial f}{\partial Yp}}{\alpha+\beta\frac{\partial Bp}{\partial Ap}}dYp \tag{S33}$$

$$dAp = -\frac{\frac{\partial f}{\partial Yp}\frac{\partial Yp}{\partial Z}}{\alpha+\beta\frac{\partial Bp}{\partial Ap}}dZ \tag{S34}$$

$$dAp = -\frac{\beta}{\alpha+\beta\frac{\partial Bp}{\partial Ap}}dBp \tag{S35}$$

The numerator of Eqs. (S32-S34), are the same for the topology with additional feedback (Fig. 1c, 1d) and without (Fig. 1a, 1b). Thus, deviations from the optimal value of $CheAp$ arising through fluctuations of total proteins concentrations get attenuated by the additional feedback loop via CheB phophorylation.

In Eq.(S35), the value for $\beta = \partial f/\partial T_A \cdot \partial T_A/\partial Bp$, in the simpler systems (Fig. 1a, 1b) is different to the systems with additional feedback, $\beta = \partial f/\partial T_A \cdot \partial T_A/\partial Bp + \partial f/\partial Bp\,|_{T_A}$. In section 3.3 we show that, for $\beta < 0$, the absolute value of the numerator for the systems with additional feedback is always smaller than for simpler systems. Thus, also in Eq. (S35) the systems with additional feedback loop are more robust.

3.1 Derivation of the condition for $\alpha < 0$

In this section we derive the condition that has to be fulfilled for α to be negative.

$$\begin{aligned}\alpha &= \left.\frac{\partial f}{\partial Ap}\right|_{T_A, Yp, Bp} + \frac{\partial f}{\partial Yp}\frac{\partial Yp}{\partial Ap} \\ &= -k_A\,T_A - k_Y\,(Y^T - Yp\,) - k'_B\,(B^T - Bp\,) + k_Y\,Y^T\,\frac{k_Y Ap\,k_Z Z}{(k_Y Ap\,+k_Z Z)^2} < 0\end{aligned}$$

Since the phosphorylation of $CheA$ is the rate limiting step in this reaction, $k_Y\,Y^T \gg k_A\,T_A$, [2]. Also, since $k_Y\,Y^T \gg k'_B\,B^T$, we can neglect the term $k'_B\,(B^T - Bp\,)$. Both simplification are conservative, i.e. they make the inequality even more strict. We get as a condition for $\alpha < 0$:

$$\begin{aligned}& -k_Y\,(Y^T - Yp\,) + k_Y\,Y^T\,\frac{k_Y Ap\,k_Z Z}{(k_Y Ap\,+k_Z Z)^2} < 0 \\ \Longrightarrow\quad & \frac{k_Y Ap\,k_Z Z}{(k_Y Ap\,+k_Z Z)^2} < \frac{Y^T - Yp}{Y^T} \\ \Longrightarrow\quad & \frac{\frac{k_Z Z}{k_Y Ap}}{\left(1+\frac{k_Z Z}{k_Y Ap}\right)^2} < \frac{Y^T - Yp}{Y^T}\end{aligned} \tag{S36}$$

There always exists a real number $\omega > -1$ such that $k_Z Z = (1+\omega)k_Y Ap\,$. Thus inequality (S36) can be written as:

$$\begin{aligned}& \frac{1+\omega}{(2+\omega)^2} = \frac{1+\omega}{4+4\omega+\omega^2} \leq \frac{1+\omega}{4\,(1+\omega)} = \frac{1}{4} < \frac{Y^T - Yp}{Y^T} \\ \Longrightarrow\quad & Y^T < 4Y^T - 4Yp \\ \Longrightarrow\quad & Yp < \frac{3}{4}Y^T\end{aligned}$$

Thus α is always negative for $Yp < 0.75\,Y^T$.

3.2 Derivation of the condition for $\beta < 0$

From Eqs. (S32)-(S35) we can see that the error reduction mechanism of the chemotaxis topology works more efficiently if the denominator increases in magnitude. Since $\partial Bp\,/\partial Ap$ is positive and α is negative, β has to be smaller

than zero for the additional feedback to have a positive noise reduction effect. Here we derive the conditions for β being smaller than zero:

$$\beta = \frac{\partial f}{\partial T_A}\frac{\partial T_A}{\partial Bp} + \left.\frac{\partial f}{\partial Bp}\right|_T = k_A\left(A^T - Ap\right)\frac{\partial T_A}{\partial Bp} + k'_B\,Ap < 0$$

From Eq.(S22) one can see that $\frac{\partial T_A}{\partial Bp} < 0$, thus we have $\frac{\partial T_A}{\partial Bp} = -\left|\frac{\partial T_A}{\partial Bp}\right|$ and we get:

$$\left|\frac{\partial T_A}{\partial Bp}\right| = \frac{\frac{k_B}{k_R}\frac{K_B}{R}}{\left(\frac{k_B}{k_R}\frac{Bp}{R} - 1\right)^2} = \frac{\frac{k_B}{k_R}\frac{Bp}{R}}{\left(\frac{k_B}{k_R}\frac{Bp}{R} - 1\right)^2}\frac{K_B}{Bp} > \frac{k'_B\,Ap}{k_A\left(A^T - Ap\right)} \tag{S37}$$

Defining $\epsilon := k'_B Ap\,/(k_A(A^T - Ap)) \approx k'_B Ap\,/(k_A A^T)$ and $\gamma := k_B Bp\,/k_R R$ we get:

$$\begin{aligned} & \frac{\gamma}{(\gamma-1)\,2}\frac{K_B}{Bp} > \epsilon \\ \iff \quad & K_B > \epsilon\,Bp\,\frac{(\gamma-1)\,2}{\gamma} \end{aligned} \tag{S38}$$

From our simulations we have $\epsilon \approx 0.014$, as well as $(\gamma-1)2/\gamma \approx 7.5$ and $Bp \approx 0.09\mu M$. Thus for K_B larger than $0.01\mu M$ we can satisfy the condition $\beta < 0$.

3.3 Derivation of the condition for $|\beta| < \left|\frac{\partial f}{\partial T_A}\frac{\partial T_A}{\partial Bp}\right|$

So far we have shown that the absolute value of the denominator of Eqs. (S32)-(S35) is larger for the topology with additional feedback than for the ones without. In order for the additional feedback to be error reducing also for the case of variations in [CheB] is that the numerator of Eq. (S35) is smaller for the topology with additional feedback. Thus we want to show:

$$\left|\frac{\partial f}{\partial T_A}\frac{\partial T_A}{\partial Bp} + \left.\frac{\partial f}{\partial Bp}\right|_T\right| < \left|\frac{\partial f}{\partial T_A}\frac{\partial T_A}{\partial Bp}\right| \tag{S39}$$

From Eqs.(S22) and (S26) we get:

$$\left.\frac{\partial f}{\partial Bp}\right|_T > 0 \qquad \frac{\partial f}{\partial T_A}\frac{\partial T_A}{\partial Bp} < 0 \tag{S40}$$

Since these two terms have opposite signs, it is sufficient to show that

$$\begin{aligned} & \left| \frac{\partial f}{\partial Bp} \bigg|_T \right| < \left| \frac{\partial f}{\partial T_A} \frac{\partial T_A}{\partial Bp} \right| \\ \iff & \left| \frac{\partial f}{\partial Bp} \bigg|_T \right| - \left| \frac{\partial f}{\partial T_A} \frac{\partial T_A}{\partial Bp} \right| = \frac{\partial f}{\partial Bp} \bigg|_T + \frac{\partial f}{\partial T_A} \frac{\partial T_A}{\partial Bp} = \beta < 0 \end{aligned} \tag{S41}$$

In section 3.2 we showed that for K_B sufficiently large, β is smaller than zero. Thus for K_B larger than a fixed lower bound, the additional feedback is attenuating the effect of gene expression noise on the kinase activity (CheAp) for any protein involved in the chemotaxis pathway.

3.4 Condition for the effectiveness of the feedback

From Eqs.(S32)-(S35) we can see that the error reduction mechanism works better the larger the term $\beta\,\partial Bp\,/\partial Ap$ gets. For $\beta\,\partial Bp\,/\partial Ap$ we can write:

$$\begin{aligned}
\beta\frac{\partial Bp}{\partial Ap} &= \left(\frac{\partial f}{\partial T_A}\frac{\partial T_A}{\partial Bp} + \left.\frac{\partial f}{\partial Bp}\right|_T\right)\frac{\partial Bp}{\partial Ap} \\
&= \left(-k_A\left(A^T - Ap\right)\frac{\frac{k_B}{k_R}\frac{Bp}{R}}{\left(\frac{k_B}{k_R}\frac{Bp}{R}-1\right)^2}\frac{K_B}{Bp} + k'_B\,Ap\right) \times \frac{k'_B\gamma_B B^T}{\left(k'_B\,Ap\,+\gamma_B\right)^2} \\
&= \left(-\mu\frac{\chi Bp}{\left(\chi Bp\,-1\right)^2}\frac{1}{Bp} + \nu\right)\kappa B^T, \qquad \text{(S42)}
\end{aligned}$$

where all greek letters are independent of Bp:

$$\begin{aligned}
\chi &= \frac{k_B}{k_R R} \\
\mu &= k_A\left(A^T - Ap\right)K_B \\
\nu &= k'_B\,Ap \\
\kappa &= \frac{k'_B\gamma_B}{\left(k'_B Ap\,+\gamma_B\right)^2}
\end{aligned}$$

The error correction mechanism performed by the feedback is stronger the larger the absolute value of Eq.(S42) is. In section 3.2 we showed that $\beta < 0$. Thus the negative term in Eq.(S42) is the dominating term. The value of the term χBp is fixed by the condition in Eq.(S22). This is necessary for the system to be able to respond to changes in concentration of the ligand. Since all variables denoted by greek letters are independent of Bp and χBp is fixed, the term in Eq.(S42) increases with B^T/Bp. Thus the smaller Bp compared to B^T, the better the error correction mechanism of the additional feedback.

References

[1] Barkai, N. and Leibler, S. Robustness in simple biochemical networks. *Nature* **387**, 913–917 (1997).

[2] Sourjik, V. and Berg, H. C. Receptor sensitivity in bacterial chemotaxis. *Proc Natl Acad Sci USA* **99**, 123–127 (2002).

[3] Rao, C. V., Kirby, J. R., and Arkin, A. P. Design and diversity in bacterial chemotaxis: a comparative study in E. coli and Bacillus Subtilis. *PLoS Biology* **2**, 239–251 (2004).

[4] Levit, M. N. and Stock, J. B. Receptor methylation controls the magnitude of stimulus-response coupling in bacterial chemotaxis. *J. Biol. Chem.* **277**, 36760–36765 (2002).

[5] Rao, C. V., Frenklach, M., and Arkin, A. P. An allosteric model for transmembrane signaling in bacterial chemotaxis. *J. Mol. Biol.* **343**, 291–303 (2004).

[6] Bray, D., Levin, M. D., and Morton-Firth, C. J. Receptor clustering as a cellular mechanism to control sensitivity. *Nature* **393**, 85–88 (1998).

[7] Sourjik, V. and Berg, H. C. Functional interactions between receptors in bacterial chemotaxis. *Nature* **428**, 437 (2004).

[8] Wadhams, G. H. and Armitage, J. P. Making sense of it all: Bacterial chemotaxis. *Nature Reviews* **5**, 1024–1037 (2004).

[9] Mello, B. A. and Tu, Y. Quantitative modeling of sensitivity in bacterial chemotaxis: The role of coupling among differnt chemoreceptor species. *Proc. Natl. Acad. Sci. U S A* **100**, 8223–8228 (2003).

[10] Shi, Y. and Duke, T. Cooperative model of bacterial sensing. *Phys. Rev. E* **58**, 6399–6406 (1998).

[11] Li, M. and Hazelbauer, G. L. Cellular stoichiometry of the components of the chemotaxis signaling complex. *J. Bacteriol.* **186**, 3687–3694 (2004).

[12] Sourjik, V. and Berg, H. C. Binding of the Escherichia coli response regulator CheY to its target measured *in vivo* by fluorescence resonance energy tranfer. *Proc. Natl. Acad. Sci. U S A* **99**, 12669–12674 (2002).

[13] Sourjik et al., in preparation.

[14] Swain, P. S. Efficient attenuation of stochasticity in gene expression trough post-transcriptional control. *J. Mol. Biol.* **344**, 965–976 (2004).

[15] http://www.anat.cam.ac.uk/ comp-cell/.

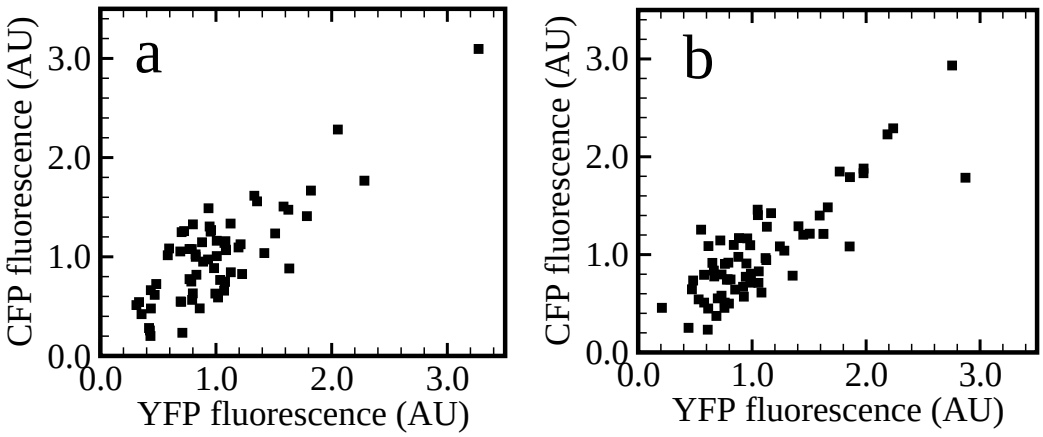

Figure S1: Single-cell levels of CheY-YFP and CheZ-CFP co-expressed from a single IPTG-inducible promoter (pVS88). **a**, Mean expression level in absence of IPTG. **b**, gene expression noise generated *in silico* by Eq. (S6) with $\nu = 0.2$ and $\alpha = 0.2$.

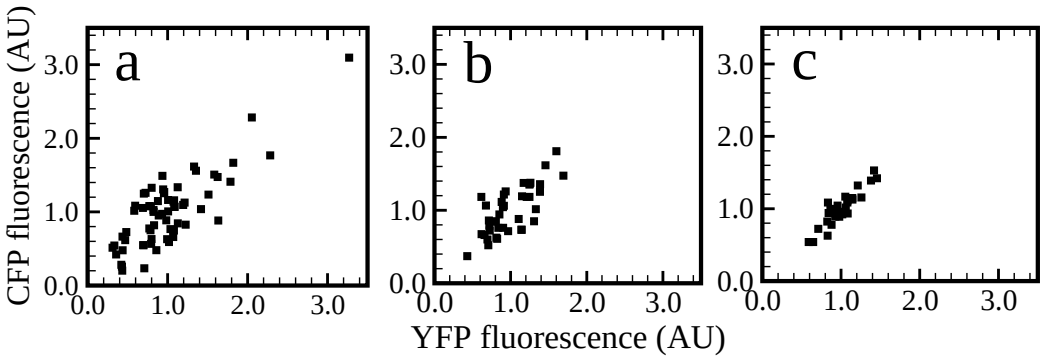

Figure S2: Gene expression noise of CheY-YFP and CheZ-CFP co-expressed from pVS88 as in Fig. 1S at 0μM (**a**), 5μM (**b**), and 10μM (**c**) IPTG. Fluorescence values for each induction level are normalized to the mean expression levels, 1, 2.5, and 14, respectively. The corresponding values for intrinsic and extrinsic noise are given in Table 1.